A Novel Mechanism for *Clostridium botulinum* Neurotoxin Inhibition†

Subramaniam Eswaramoorthy, Desigan Kumaran, and Subramanyam Swaminathan*

Biology Department, Brookhaven National Laboratory, Upton, New York 11973

Received January 18, 2002; Revised Manuscript Received May 24, 2002

ABSTRACT: *Clostridium botulinum* neurotoxins are zinc endopeptidase proteins responsible for cleaving specific peptide bonds of proteins of neuroexocytosis apparatus. The ability of drugs to interfere with toxin's catalytic activity is being evaluated with zinc chelators and metalloprotease inhibitors. It is important to develop effective pharmacological treatment for the intact holotoxin before the catalytic domain separates and enters the cytosol. We present here evidence for a novel mechanism of an inhibitor binding to the holotoxin and for the chelation of zinc from our structural studies on *Clostridium botulinum* neurotoxin type B in complex with a potential metalloprotease inhibitor, bis(5-amidino-2-benzimidazolyl)methane, and provide snapshots of the reaction as it progresses. The binding and inhibition mechanism of this inhibitor to the neurotoxin seems to be unique for intact botulinum neurotoxins. The environment of the active site rearranges in the presence of the inhibitor, and the zinc ion is gradually removed from the active site and transported to a different site in the protein, probably causing loss of catalytic activity.

Clostridium botulinum, a Gram-positive spore-forming bacterium, produces seven serotypes (A−G) of botulinum neurotoxins (BoNTs)[1] which are solely responsible for botulism causing flaccid paralysis and death (*1*, *2*). The intoxication by neurotoxins is proposed to be a four-step process (*3*−*6*): (1) cell binding, (2) internalization, (3) translocation into cytosol, and (4) enzymatic modification of a cytosolic target. The toxin first binds to the neuronal cell and then is internalized into the vesicles. To attack the targets in cytosol the neurotoxin should cross the hydrophobic barrier of the vesicle membrane. This is common to all bacterial toxins with intracellular targets and is the least understood step in the process. It is proposed that the acidification of the vesicle lumen by a proton pumping ATPase leads to conformational changes in the toxin. The acidic conformation then exposes a hydrophobic area of the toxin molecule, creates an ion channel in the membrane, and inserts the light chain (LC) into cytosol (*4*, *7*). However, not all internalized toxin molecules are translocated, the limiting factor being the reduction of the disulfide bond between heavy and light chains (*8*). Those toxin molecules not translocated are degraded in the acidic compartments. The three-dimensional structures of BoNT/A and B reveal the three structural domains corresponding to the three functions, viz., binding, translocation, and catalytic activity (*5*, *9*−*11*). The crystal structure of BoNT/B light chain with its substrate peptide fragment reveals the mode of binding of the substrate (*12*). All serotypes contain a zinc-binding motif HExxH in their catalytic domain, and their three-dimensional structures are expected to be similar in general because of significant sequence homology (*13*). However, structural details may be different, as seen between BoNT/A and BoNT/B, because of the specificity of the substrate and the scissile bond to be cleaved (*14*−*20*). The catalytic zinc is located in a deep cavity in the active site that has a wide opening for the substrate or inhibitor to enter the site. However, the deep cavity is partially covered by the belt region in BoNT/A while it is open in BoNT/B.

As of now, the treatment for botulism is a preventive one, an experimental vaccine, but no specific drug has been developed for treatment after being afflicted by botulism. Therapeutic treatments could be effective at any one of the three stages of toxicity—binding of toxin or internalization or catalytic activity (*11*). Since chelation of zinc antagonizes the neuromuscular blocking properties of botulinum neurotoxins (*21*), specific zinc chelators or inhibitors of zinc metalloproteases are being evaluated (*22*). Recently, a coumarin derivative has been tested on the light chain of botulinum neurotoxin B (*23*). Bis(5-amidino-2-benzimidazolyl)methane (BABIM), an effective zinc chelator (*24*), has been tested with BoNT/B light chain, and its IC50 (inhibition constant) is in the range of 5−10 μM (Michael Adler, personal communication). However, its effectiveness on the holotoxin is still to be studied. The crystal structure of BABIM in complex with the light chain of BoNT/B (BoNT/B-LC) has been reported (*25*). Here we present the crystal structure of a protein−inhibitor complex of intact botulinum neurotoxin type B and BABIM determined at different durations of soaking to understand the mechanism of inhibition and the probable path of entry for the inhibitor. These structures provide a series of snapshots during the reaction and reveal a possible mechanism of binding and chelation of the zinc ion.

† Research supported by the Chemical and Biological Nonproliferation Program NN20 of the U.S. Department of Energy and the U.S. Army Medical Research Acquisition Activity (Award No. DAMD17-02-2-0011) under Prime Contract No. DE-AC02-98CH10886 with Brookhaven National Laboratory. D.K. was partly supported by funds from Veterans Administration Medical Center, Pittsburgh.

* To whom correspondence should be addressed. Telephone: (631) 344-3187. Fax: (631) 344-3407. E-mail: swami@bnl.gov.

[1] Abbreviations: BoNT, botulinum neurotoxin; LC, light chain; BABIM, bis(5-amidino-2-benzimidazolyl) methane; NSLS, the National Synchrotron Light Source.

10.1021/bi020060c CCC: $22.00 © 2002 American Chemical Society
Published on Web 07/13/2002

Table 1: Crystal Data and Refinement Statistics

cell parameters: $a = 75.92$, $b = 123.24$, $c = 95.90$ Å, and $\beta = 113.7$ °. space group $P2_1$				
PDB idcode	1G9B	1G9D	1G9A	1G9C
		Data Collection		
soaking time (min)	2	4	12	20
resolution (Å)	50.0−1.9	50.0−2.2	50.0−2.0	50.0−2.35
total number of reflections	297 330	295 435	308 578	224 958
number of unique reflections	104 669	81 518	95 973	64 852
completeness[a] (%)	82.7 (18.4)	97.4 (92.0)	84.5 (16.1)	98.6 (91.0)
R_{merge}[b] (R_{merge} last shell)	0.062 (0.45)	0.064 (0.38)	0.063 (0.46)	0.058 (0.35)
$\langle I/\sigma(I)\rangle$	12.5	12.6	9.7	10.6
		Refinement		
resolution (Å)	50.0−2.0	50.0−2.2	50.0−2.1	50.0−2.35
number of reflections (overall completeness)	93 756 (86.3)	69 919 (90.7)	83 496 (88.8)	60 645 (93.1)
$F/\sigma(F)$ cutoff value	0	0	0	0
R_{free}[c]	0.243	0.283	0.248	0.247
R_{work}[c]	0.213	0.263	0.213	0.210
RMSD				
bond lengths (Å)	0.007	0.007	0.007	0.007
bond angles (deg)	1.37	1.44	1.38	1.40
number of atoms				
protein	10 587	10 587	10 587	10 587
water molecules	548	383	546	422
inhibitor	50	50	50	50
Zn (partially occupied)	2	2	2	2
occupancy of Zn1 (B Å^2)	0.65(51.1)	0.59(61.5)	0.56(59.3)	0.50(54.1)
occupancy of Zn2 (B Å^2)	0.35(50.3)	0.41(71.1)	0.44(59.8)	0.50(56.4)
$\langle B\rangle$ protein (Å^2)	29.6	30.6	31.0	31.9

[a] Completeness for the highest bin is given within parentheses. Outermost shell: 2.02−1.9 (1G9B), 2.28−2.20 (1G9D), 2.13−2.0 (1G9A), and 2.43−2.35 (1G9C). [b] $R_{merge} = \Sigma_j(|I_h - \langle I\rangle_h|)/\Sigma I_h$, where $\langle I_h\rangle$ is the average intensity over symmetry equivalents. [c] $R = \Sigma|F_{obs} - F_{calc}|/\Sigma|F_{obs}|$; R_{work} is summed over reflections used in refinement, and R_{free} is summed over reflections set aside for validation.

MATERIALS AND METHODS

Preparation of Protein for Crystallization. Intact neurotoxin was purchased from the Food Research Institute (Madison, WI). Since the BoNT endopeptidase activity is expressed only after the disulfide bond is reduced (*26*), preparation of protein for crystallization was slightly modified from the published procedure (*27*). Also, because the protein is supplied as a precipitate in ammonium sulfate, a sulfate ion was found to be present in the catalytic site (*10*). Since the sulfate ion might possibly hinder inhibitor binding, the sulfate ion was removed before crystallization. The protein was dialyzed against 100 mM NaCl, 50 mM Hepes, and 10 mM dithiothreitol at pH 7.0 overnight in two steps. Then 80 mM barium acetate was added to the dialysate to remove the sulfate ion bound in the catalytic site and dialyzed twice again. The final dialysis was done without barium acetate. Crystallization condition is as described but under reducing condition (*27*).

Inhibitor Soaking. Initially, various concentrations of BABIM and durations of soaking were tried to test the stability of the crystal and its diffraction quality. The optimum concentration of BABIM for soaking was determined as 3 mM, since at higher concentrations the crystals dissolved within a short duration of soaking or the crystal quality became extremely poor and at lower concentrations BABIM could not be seen in the electron density maps. Because the goal was to study the inhibition mechanism, crystals were soaked for different duration. Crystals were soaked for 2, 4, 12, and 20 min in the cryoprotectant solution containing BABIM and immediately frozen to liquid nitrogen temperature, by plunging the crystal into a vial of liquid nitrogen, to stop the reaction. For soaking durations larger than 20 min, either the crystals dissolved or the diffraction was extremely poor. Neither varying the molecular weight of the precipitant (PEG) nor increasing the precipitant concentration helped.

Data Collection. Data were collected at liquid nitrogen temperature at the x12C beamline of the NSLS, Brookhaven National Laboratory with Brandeis CCD based B1 detector. An oscillation range of 1° was used for each data frame, and data corresponding to 200° in ϕ were collected with crystal to detector distance of 100 mm and $\lambda = 1.01$ Å. Data were reduced with DENZO and SCALEPACK (*28*). Data collection statistics are presented in Table 1. In the case of two data sets, a resolution cutoff has been used in the refinement since the completion in the highest resolution shell was less than 20% and R_{merge} was high.

Structure Determination. Initial model coordinates were obtained from PDB idcode 1epw. After initial rigid body refinement, the structures were refined with CNS (*29*). Adjustments of the original model was done with 'O' (*30*). The protein model is complete except for residues 440, 441, and 442, which are in the proteolytic site. A σA-weighted Fo−Fc map was calculated with refined models, and clear continuous residual density could be seen for the inhibitor molecules (Figure 1a,b). The starting model for BABIM was taken from Katz et al. (*24*). The model was further refined with the inhibitor and water molecules included. Refinement statistics are included in Table 1. Structures were validated with PROCHECK (*31*).

RESULTS AND DISCUSSION

Description of the Structure. Two inhibitor molecules are bound to the holotoxin and give a clue to probable pathways

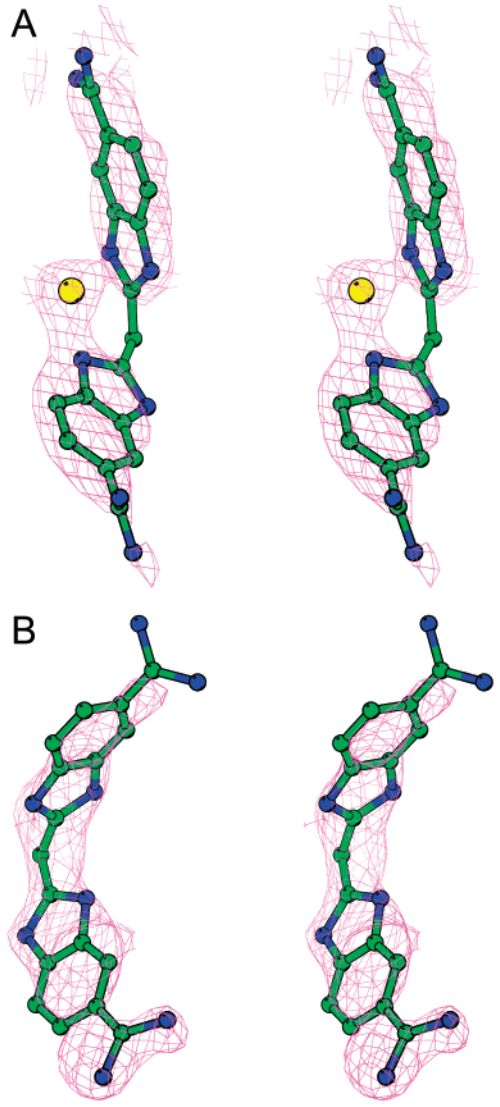

FIGURE 1: Stereoview of 2Fo−Fc maps. σA-weighted 2Fo−Fc maps superposed on the refined positions of BABIM1 (a) and BABIM2 (b). Contours are drawn at 1σ. Zinc atom bound to BABIM is shown in yellow. The density is weak for C9 of BABIM1 and for N1 and N2 of BABIM2.

for them to enter the active site (Figure 2a−c). A cleft formed between the translocation domain and the catalytic domain is connected to the active site cavity (cavity 1), and both of them form part of a tunnel (Figure 2b,c). This tunnel is lined by negatively charged atoms and accordingly has a negative electrostatic potential. Asp 375 of the catalytic domain lies midway in this tunnel and is hydrogen bonded to Thr 713 through a water molecule and acts like a gate (Figure 3a,b). Interestingly, this network of hydrogen bonds separates the two BABIM molecules, suggesting that there are two pathways for the inhibitor to enter the molecule (Figure 2b,c). It is proposed that one inhibitor molecule (BABIM2) has entered through this cleft between the translocation and catalytic domains. Since Asp 375 prevents it from moving through the channel any further, it stays there because of favorable interactions.

Inhibitor Binding Sites. Inhibitor molecule BABIM2 sits in the cleft formed between the translocation and binding domains and makes contacts with both the catalytic and translocation domains. The inhibitor is near residue Lys 720 and Asp 375 (Figure 3c). The side chains of residues Asp 375 and Lys 720 interact with the π-electron clouds of one of the benzimidazolyl groups. Nζ of Lys 720 also makes hydrogen bond with N4′ of BABIM2. N1 and N2 of the inhibitor make hydrogen bonds with NH2 of Arg 217 and Nδ2 of Asn 203. N3 and N4′ make hydrogen bonds with Oδ1 of Asp 452. N3′ of the benzimidazolyl group makes hydrogen bond with O of Asp 452. N2′ interacts with O of Asp 447 through a water molecule besides hydrogen bonding to O of Phe 537. N1′ interacts with the OH of Tyr 724. The hydrogen-bonding contacts are listed in Table 2.

When the catalytic domain (L chain) is considered in isolation along with the belt region, one more cavity (cavity 2) in addition to the deep and wide open active site cavity (cavity 1) could be identified (Figure 2c). Residues 373−375 and 454−457 are along the opening of this cavity. At the bottom, this cavity opens up into the active site cavity, and hence there is a continuous channel from the active site cavity up to the top of cavity 2. However, when the holotoxin is considered as a whole, part of one of the long α helices (residues 709−713) is up against this opening, transforming it into a small pocket. This pocket becomes part of the tunnel. The inhibitor molecule, BABIM1, enters this pocket, presumably through the wide opening of the active site cavity and stays bound to the protein (Figure 3a,b). One of the amidino groups interacts with the active site residues, while the other amidino group nitrogens make many contacts with the translocation domain. One of the amidino groups of BABIM1 is between Arg 369 and Tyr 372. N1 of the amidino group hydrogen bonds to NH1 of Arg 369. The benzimidazole nitrogen atoms N3 and N4 are making hydrogen bonds with catalytic domain. N3 makes hydrogen bond to Oδ1 of Asp 68, and N4 makes hydrogen bonds with O of Ser 374 and Oγ of Ser 376. N4′ of BABIM1 interacts with Oϵ1, O, and Oδ1 of Gln 258, Glu 451, and Asp 375, respectively. N1′ and N2′ of the other amidino group interact with the translocation domain. N1′ is hydrogen bonded to Oγ1 of Thr 713. N2′ is hydrogen bonded to O and Oγ1 of Thr 709 and O of Phe 455.

Perturbation of the Active Site. The active site has been mapped in the structure of holotoxin BoNT/B determined to 1.7 Å resolution (S. Eswaramoorthy and S. Swaminathan, unpublished data). The zinc ion in the active site is coordinated to residues His 229, His 233, Glu 267, and a water molecule. The inhibitor molecules in the present structure do not stay bound to Zn through coordination, as observed in serine proteases and in BoNT/B-LC:BABIM complex (*24*, *25*). However, the active site environment in the present structure is perturbed, probably due to the presence of BABIM (Figure 4). Significantly, the coordination between the Zn and Glu 267 is lost, and the side chain of Glu 267 takes a different rotamer position to make a hydrogen bond to Gln 264 (Table 2). The inhibitor might be competing with Glu 267 for a possible coordination to Zn. A composite-omit map shows a water molecule in the place of Oϵ1 of Glu 267 coordinating to Zn besides the presumed nucleophilic water. This water molecule is hydrogen bonded to Zn and the carbonyl oxygen of Glu 267. The nucleophilic water molecule coordinating with Zn is making a hydrogen bond to Oϵ2 of Glu 230. The water molecules are 2.4 and 2.6 Å away from the Zn; also, one of the histidine

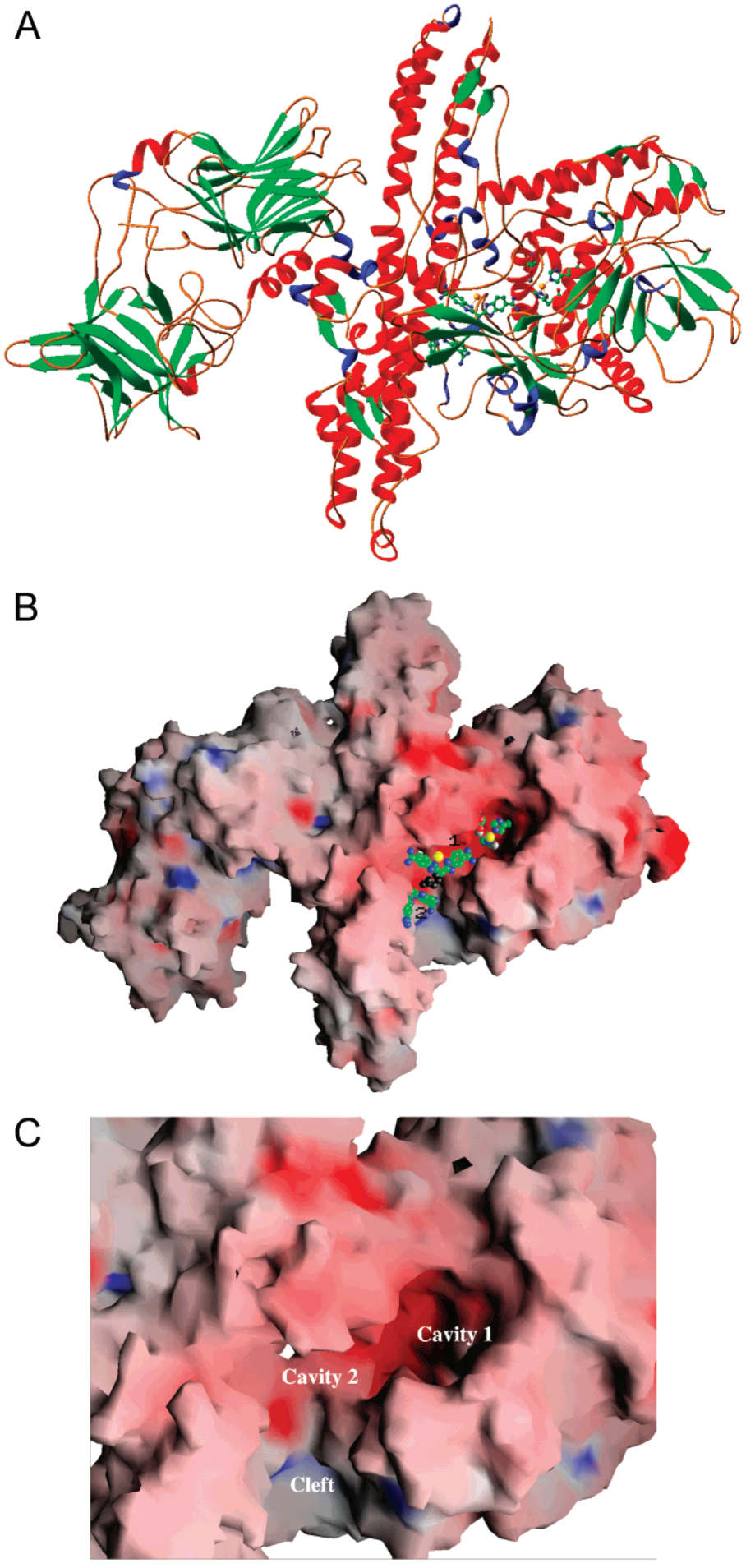
A
B
C
Cavity 1
Cavity 2
Cleft

coordination distances has become longer (2.6 Å). The coordination of the Zn and the above-mentioned residues were very strong in the holotoxin, unlike in this structure. This somewhat larger coordination distances and loss of coordination with Glu 267 make Zn binding less stable. Since Zn plays a structural role also and its removal changes the tertiary structure, the protein itself may become unstable (*32*, *33*). This may be an intermediate stage before the Zn gets removed completely and the structure collapses. This is supported by the fact that the crystal dissolves when BABIM concentration in the mother liquor is increased or if the crystal is soaked for a longer duration.

Novel Binding and Inhibition Mechanism. The catalytic domain has a wide and deep cavity at the active site. The cleavage and binding sites in the substrate are different and separated, and the binding region is essential for the cleavage of scissile bond. Though the substrate synaptobrevin is a large molecule, biochemical studies have shown that a minimum length of 51 peptides containing the binding and the cleavage regions is enough for cleavage of the substrate to take place (*34*). The substrate partly takes the position of the belt region in the crystal structure of the light chain:synaptobrevin complex and extends on both sides of the active site with the region around the scissile bond to be cleaved protruding inside the opening and approaching close to the zinc site (*12*). The substrate binds to the protein between the loops 50 and 250 where the light chain would be interacting with the translocation domain in the holotoxin. In the structures reported here, BABIM1 and 2 partially occupy the synaptobrevin site and would block the binding of the substrate to the toxin eventually blocking the cleavage activity. The binding of two inhibitor molecules to the toxin molecule reveals an unexpected binding mechanism of the inhibitor.

Residues Arg 369 and Tyr 372 are presumably involved in the protease activity (*26*). In the structure of the BoNT/B-LC:synaptobrevin complex, the cleaved residues of the substrate, synaptobrevin-II, are supposedly stabilized by the protein residues Arg 369 and Tyr 372, which suggests that spatially they must have been close to the scissile bond to be cleaved. In this structure the BABIM1 binding mimics this intermediate state of substrate binding. The amidino group lies between Arg 369 and Tyr 372 with N1 of the inhibitor hydrogen bonded to Arg 369. The catalytic activity might be blocked either by the nonavailability of this donor atom or because the substrate binding is blocked.

We propose a mechanism for zinc chelation as seen in this study. To do a time-dependent study of inhibitor binding, we soaked crystals in mother liquor containing 3 mM of the inhibitor for various periods of time, and the reaction was presumably stopped by immediately freezing the crystals to liquid nitrogen temperature. Experiments done with approximate soaking times of 2, 4, 12, and 20 min are reported in this study. Because of the disruption of the coordination, the temperature factor of the zinc ion increased with the soaking time. Simulated omit maps brought out two peaks which could be modeled as partially occupied zinc atoms—one in the original site and the other bound to BABIM1 by chelating nitrogens N3 and N3′ and to Nϵ2 of Gln 258. The combined peak heights of the partially occupied zinc atoms were comparable to that of a fully occupied zinc atom in structures of the same protein at similar resolution. Assuming that there is one zinc atom per molecule, occupancies were assigned on the basis of the relative peak heights in the difference Fourier maps. For BABIM1, occupancies were set equal to that of the bound zinc. Interestingly, as the soaking time increases, the occupancy of the original zinc

Table 2: Hydrogen Bonding and Other Interactions Involving BABIM1, BABIM2, and Zn[a]

residue	atom name	residue and atom name	distance (Å)
		BABIM1	
BAB	N1	NH1 R369	3.18
BAB	N3	OD1 D68	3.24
BAB	N4	O S374	2.63
BAB	N4	OG S376	3.40
BAB	N4′	OE1 Q258	2.54
BAB	N4′	O E451	2.64
BAB	N4′	OD1 D375	3.00
BAB	N2′	O F455	2.40
BAB	N2′	O T709	3.14
BAB	N2′	OG1 T709	2.93
BAB	N1′	OG1 T713	2.40
BAB	N3	Zn2	2.41
BAB	N3′	Zn2	2.50
Zn2		NE2 Q258	2.55
		BABIM2	
BAB	N1	NH2 R217	2.60
BAB	N2	ND2 N203	2.58
BAB	N3	OD1 D452	2.52
BAB	N4′	OD1 D452	3.18
BAB	N4′	NZ K720	3.18
BAB	N3′	O D452	2.82
BAB	N2′	O F537	2.99
BAB	N2′	O water	2.60
BAB	N1′	OH Y724	2.89
		Perturbed Active Site	
zinc	Zn	NE2 H229	2.32
zinc	Zn	NE2 H233	2.15
zinc	Zn	O water	2.40
zinc	Zn	O water	2.42
water	O	OE2 E230	3.26
water	O	O E267	2.96
E267	OE2	N Q264	2.64

[a] The high and low cutoff values used for hydrogen bond distances and angles are 3.5 Å and 120°, respectively.

FIGURE 2: (a) RIBBONS (*35*) representation of BoNT/B. Helices in blue represent 3_{10} helices. Two molecules of BABIM and the zinc site residues are shown as ball-and-stick model. The two partially occupied zinc atoms are shown in yellow, while water molecules are in silver gray. (b) Grasp (*36*) representation of the electrostatic potential surface of BoNT/B. BABIM1 and 2 trapped in the tunnel and the residues coordinating zinc are shown as sphere model. Zn atoms are shown in yellow, while water molecules coordinating with active site Zn are in silver gray. Glu 267 moves away from Zn with one of the water molecules replacing its coordination. The top of the tunnel wall is clipped for clarity by excluding residues 67−68, 253−261, 431−455, and 525−532 from the model. Asp 375 (shown in black) lies between BABIM1 and 2 (labeled as 1 and 2). The positive and negative electrostatic potentials are represented in blue and red. (c) An enlarged view of the BABIM1 and 2 binding site. BABIM1 and 2 and the active site residues shown in panel b are not included in this figure for clarity. Cavity 1 is the wide and deep active site cavity. Cavity 2 would have an opening in the isolated light chain but in intact toxin is blocked by the long helices of the translocation domain as shown here and connects cavity 1 and the cleft between the translocation and catalytic domain to form a channel.

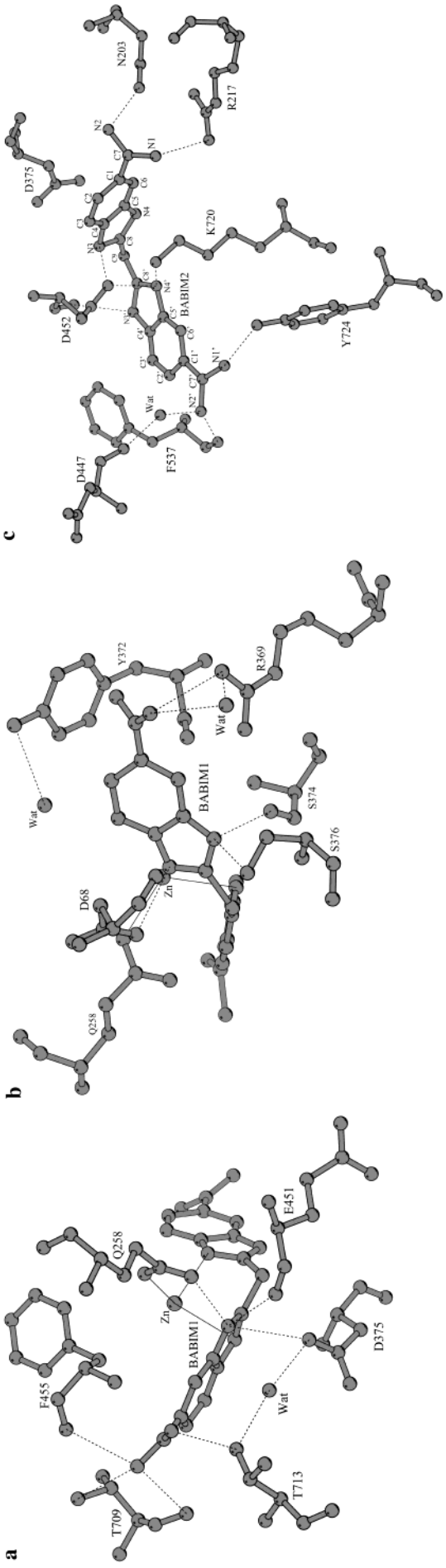

FIGURE 3: (a and b) Residues interacting with BABIM1. For clarity, residues surrounding each amidinobenzimidazolyl groups are given separately. Hydrogen bonds are shown as dashed line, while the metal coordinations are as thin solid lines. As shown here and in Table 2, BABIM1 interacts with both the translocation and catalytic domains. (c) Residues interacting with BABIM2. Hydrogen bond interactions are listed in Table 2 and shown here in dashed lines. Asp 375 and Lys 720 lie on either side of one of the benzimidazolyl group and their interactions are mostly π-interactions.

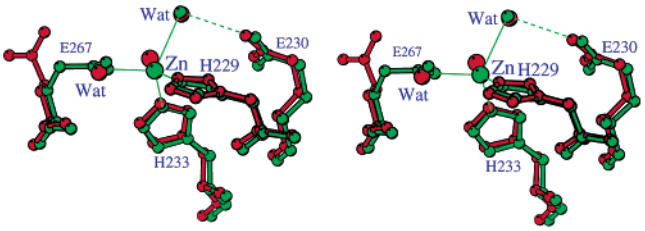

FIGURE 4: Stereoview of the superposition of the unperturbed (in green) and the perturbed states (red) of the active site. The active site residues are perturbed when crystals are complexed with BABIM. The side chain of Glu 267 takes a different orientation, and a water molecule replaces the carboxylate group. Coordinating distance between Zn and Nϵ2 of His 229 has increased to more than 2.6 Å. Figures 1, 3, and 4 were produced with MOLSCRIPT (*37*).

ion decreases, while the one bound to BABIM1 increases (Table 1). When the crystal was soaked for 1 min or less, though BABIM could not be located in the difference map, the perturbation of zinc coordination was evident (data not shown). We believe that BABIM1 binds to the zinc ion and moves it away from the active site to a position where interactions for it to bind to the protein are more favorable. Since the soaking was done for a very short duration and the crystal was flash frozen, it is possible that the reaction was not taken to completion and what we see is an average structure of a transitory state. Partial occupancy and high thermal factors for zinc ions indicate that the zinc ion has not been completely removed from the protein. Probably the reaction was halted before BABIM could attack every molecule in every unit cell of the crystal. The mode of zinc binding to BABIM1 suggests that initially BABIM1 should have bound to the active site zinc via N3 and N3′ of BABIM. However, since the experiment was done by soaking crystals in the mother liquor containing BABIM, it was not possible to see the instantaneous binding of BABIM1 to the active site zinc. Extrapolating from the conformation of BABIM1 and the bound zinc, we modeled this binding mode (Figure 5). Since Glu 267 had already taken a different rotamer position and other side chains in this region were perturbed, we could model this without disturbing the protein model. The model was built with ′O′ (*30*) and energy minimized with CNS, and it seems to be energetically favorable since the cavity is wide open. An ideal experiment would be to soak the crystal for an optimum duration for the reaction to be completed. However, this was not possible, since crystals dissolve if soaked longer in BABIM solution, suggesting that the crystal becomes unstable when zinc is removed.

In the present study, we find two BABIM molecules bound to the protein, while in the crystal structure of BoNT/B-LC with BABIM, there is only one bound BABIM since it lacks the heavy chain altogether. Also in the present study, the zinc is coordinated with N3 and N3′ of BABIM1, and the torsion angle C8−C9−C8′−N3′ is 147°, an energetically favorable conformation. In the crystal structure of BoNT/B-LC:BABIM, the zinc is coordinated with N1′ and N2′ of BABIM, and the inhibitor molecule is planar, with C8−C9−C8′−N3′ equal to 179°.

CONCLUSION

The advent of cryocrystallography has now made it possible to study the enzymatic reactions via X-ray crystal-

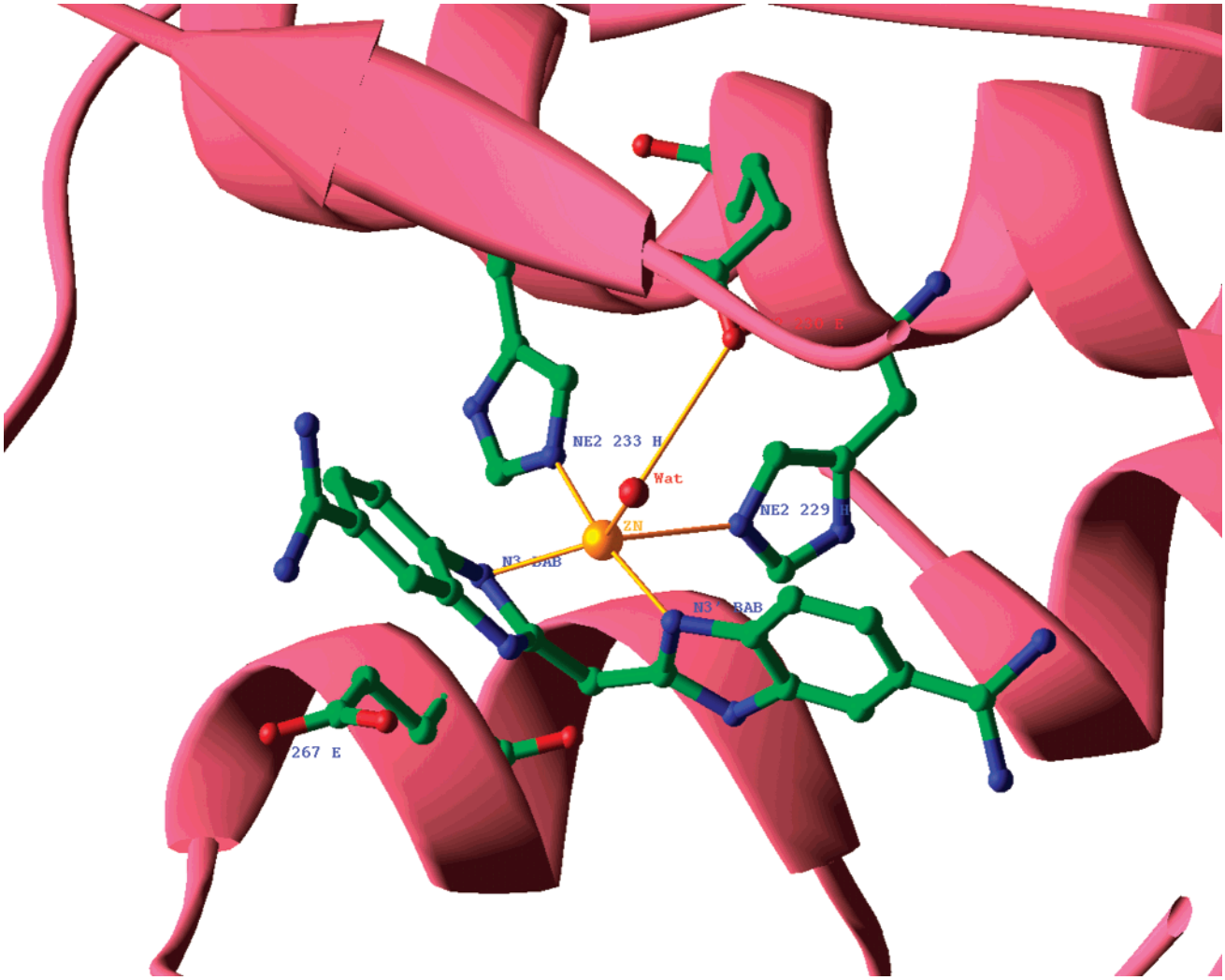

FIGURE 5: BABIM modeled at the active site is shown along with RIBBONS (*35*) representation of the light chain and the belt region. The mode of binding of zinc was assumed to be similar to that of BABIM1. There was no disruption to the active site, since the perturbation of the side chains is already taken into consideration and the side chain of Glu 267 has already moved away from zinc. This model is similar to Katz et al. (*24*). Coordination to zinc ion from protein ligands and the inhibitor are shown as thin yellow lines.

Table 3: Data Statistics for Each Data Set[a]

					1G9B					
resol. bins (Å)	50.0-4.35	3.45	3.02	2.74	2.54	2.39	2.27	2.17	2.09	2.0
completeness	99.0	99.5	99.5	99.0	97.5	96.5	94.6	89.1	80.9	65.1
R_{merge}	0.031	0.036	0.052	0.082	0.126	0.167	0.211	0.247	0.292	0.324
					1G9D					
resol. bins (Å)	50.0-4.74	3.76	3.29	2.99	2.77	2.61	2.48	2.37	2.28	2.20
completeness	98.8	99.7	99.5	99.2	98.9	98.1	96.6	96.9	96.0	92.7
R_{merge}	0.033	0.040	0.055	0.103	0.131	0.164	0.246	0.312	0.319	0.375
					1G9A					
resol. bins (Å)	50.0-4.58	3.63	3.17	2.88	2.68	2.52	2.39	2.29	2.20	2.10
completeness	99.4	100.0	100.0	100.0	100.0	100.0	99.5	95.2	85.3	70.6
R_{merge}	0.043	0.055	0.073	0.102	0.149	0.204	0.259	0.300	0.349	0.380
					1G9C					
resol. bins (Å)	50.0-5.06	4.02	3.51	3.19	2.96	2.79	2.65	2.53	2.43	2.35
completeness	100.0	100.0	100.0	100.0	99.9	99.6	99.5	99.0	96.7	91.0
R_{merge}	0.036	0.042	0.055	0.078	0.109	0.160	0.216	0.276	0.332	0.352

[a] For 1G9B and 1G9A, the completeness and the R_{merge} for the resolution bin not used in the refinement are given in Table 1.

lography, though with some limitations, and we have used this technique to study the inhibition mechanism as a function of time. In summary, the structure of BoNT/B in complex with an inhibitor, BABIM, shows that the active site residues rearrange in the presence of the inhibitor and the active site zinc is progressively removed. The inhibitor partly occupies the site where the substrate would bind and blocks it from binding to the toxin. We have also shown that it is possible for appropriate inhibitors to enter the active site of the holotoxin. However, the inhibition could be due to either the nonavailability of substrate-binding sites or the removal of zinc or a combination of both.

APPENDIX

Coordinates. Atomic coordinates have been deposited in the Protein Data Bank. Accession codes are 1G9A, 1G9B, 1G9C, and 1G9D, as given in Table 3.

ACKNOWLEDGMENT

We thank Drs. D. H. Rich and T. Oast, University of Wisconsin, for the generous gift of BABIM and Drs. M. Adler and B. R. Singh for useful discussions. We thank the reviewers for their helpful comments.

REFERENCES

1. Sathyamurthy, V., and Dasgupta, B. R. (1985) *J. Biol. Chem. 260*, 10461−10466.
2. Schiavo, G., Matteoli, M., and Montecucco, C. (2000) *Physiol. Rev. 80*, 717−766.
3. Schantz, E. J., and Johnson, E. A. (1992) *Microbiol. Rev. 56*, 80−99.
4. Menestrina, G., Schiavo, G., and Montecucco, C. (1994) *Mol. Aspects Med. 15*, 79−193.
5. Montecucco, C., and Schiavo, G. (1994) *Mol. Microbiol. 13*, 1−9.
6. Oguma, K., Fujinaga, Y., and Inoue, K. (1995) *Microbiol. Immunol. 39*, 161−168.
7. Schiavo, G., Rossetto, O., and Montecucco, C. (1994) *Semin. Cell Biol. 5*, 221−229.
8. de-Paiva, A., Poulain, B., Lawrence, G. W., Shone, C. C., Tauc, L., and Dolly, J. O. (1993) *J. Biol. Chem. 268*, 20838−20844.
9. Lacy, D. B., Tepp, W., Cohen, A. C., DasGupta, B. R., and Stevens, R. C. (1998) *Nat. Struct. Biol. 5*, 898−902.
10. Swaminathan, S., and Eswaramoorthy, S. (2000) *Nat. Struct. Biol. 7*, 693−699.
11. Montecucco, C., Papini, E., and Schiavo, G. (1994) *FEBS Lett. 346*, 92−98.
12. Hanson, M. A., and Stevens, R. C. (2000) *Nat. Struct. Biol. 7*, 687−692.
13. Schiavo, G., Rossetto, O., Santucci, A., Dasgupta, B. R., and Montecucco, C. (1992) *J. Biol. Chem. 267*, 23479−27483.
14. Schiavo, G., Shone, C. C., Rossetto, O., Alexander, F. C. G., and Montecucco, C. (1993) *J. Biol. Chem. 268*, 11516−11519.
15. Schiavo, G., Benfenati, F., Poulain, B., Rossetto, O., de-Lauretto, P. P., Dasgupta, B. R., and Montecucco, C. (1992) *Nature 359*, 832−835.
16. Blasi, J., Chapman, E. R., Yamasaki, S., Binz, T., Niemann, H., and Jahn, R. (1993) *EMBO J. 12*, 4821−4828.
17. Schiavo, G., Santucci, A., Dasgupta, B. R., Metha, P. P., Jontes, J., Benfenati, F., Wilson, M. C., and Montecucco, C. (1993) *FEBS Lett. 335*, 99−103.
18. Schiavo, G., Rossetto, O., Catsicas, S., Polverino-de-Laureto, P., Dasgupta, B. R., Benfenati, F., and Montecucco, C. (1993) *J. Biol. Chem. 268*, 23784−23787.
19. Schiavo, G., Malizio, C., Trimble, W. S., Polverino-de-Laureto, P., Milan, G., Sugiyama, H., Johnson, E. A., and Montecucco, C. (1994) *J. Biol. Chem. 269*, 20213−20216.
20. Söllner, T., Whiteheart, S. W., Brunner, M., Erdjument-Bromage, H., Geromanos, S., Tempst, P., and Rothman, J. E. (1993) *Nature 362*, 318−324.
21. Simpson, L. L., Coffield, J. A., and Bakry, N. (1993) *J. Pharmacol. Exp. Ther. 267*, 720−727.
22. Auld, D. S. (1995) *Methods Enzymol. 248*, 228−242.
23. Adler, M., Nicholson, J. D., and Hackley, B. E. (1998) *FEBS Lett. 429*, 234−238.
24. Katz, B. A., Clark, J. M., Finer-Moore, J. S., Jenkins, T. E., Johnson, C. R., Ross, M. J., Luong, C., Moore, W. R., and Stroud, R. M. (1998) *Nature 391*, 608−612.
25. Hanson, M. A., Oost, T. K., Sukonpan, C., Rich, D. H., and Stevens, R. C. (2000) *J. Am. Chem. Soc. 122*, 11268−11269.
26. Li, L., Binze, T., Niemann, H., and Singh, B. R. (2000) *Biochemistry 39*, 2399−2405.
27. Swaminathan, S., and Eswaramoorthy, S. (2000) *Acta Crystallogr., Sect. D 56*, 1024−1026.
28. Otwinowski, Z., and Minor, W. (1997) *Methods Enzymol. 276*, 307−326.
29. Brunger, A. T., Adams, P. D., Clore, G. M., Delano, W. L., Gros, P., Grosse-Kunstleve, R. W., Jiang, J. S., Kuszwewski, J., Nilges, M., Pannu, N. S., Read, R. J., Rice, L. M., Somonsom, T., and Warren, G. L. (1998) *Acta Crystallogr., Sect. D 54*, 905−921.
30. Jones, T. A., Zou, J., Cowtan, S., and Kjeldgaard, M. (1991) *Acta Crystallogr., Sect. A 47*, 110−119.
31. Laskowski, R. A., MacArthur, M. W., Moss, D. S., and Thornton, J. M. (1993) *J. Appl. Crystallogr. 26*, 283−291.
32. Fu, F., Lomneth, R. B., Cai, S., and Singh, B. R. (1998) *Biochemistry 37*, 5267−5278.
33. Li, L., and Singh, B. R. (2000) *Biochemistry 39*, 10581−10586.
34. Foran, P., Shone, C. C., and Dolly, J. O. (1994) *Biochemistry 33*, 15365−15374.
35. Carson, M. (1991) *J. Appl. Crystallogr. 24*, 958−961.
36. Nicholls, A., Sharp, K., and Honig, B. (1991) *Proteins 11*, 281−296.
37. Kraulis, P. J. (1991) *J. Appl. Crystallogr. 24*, 946−950.

BI020060C